UNIVERSITY OF CALIFORNIA SAN DIEGO

Experimental Studies of Nonlinear Electron Acoustic Waves

A thesis submitted in partial satisfaction of the
requirements for the degree
Master of Science

in

Physics

by

Jacob Stone Saret

Committee in charge:

Professor C. Fred Driscoll, Chair
Professor Daniel Dubin
Professor Brian Shotwell

2023

The thesis of Jacob Stone Saret is approved, and it is acceptable in quality and form for publication on microfilm and electronically.

University of California San Diego

2023

TABLE OF CONTENTS

LIST OF FIGURES

ACKNOWLEDGEMENTS

My thanks goes to all of my colleagues in the Nonneutral Plasma group for all of the time and effort they committed to help me learn and grow as a fledgeling researcher. First, I thank my advisor Prof. C. Fred Driscoll for his encouragement to pursue my interests with constitution and passion, all his witticisms regarding both physics and life in general, and teaching me by example the fine balance of how to not let anything get by without its due diligence while always avoiding getting stuck.

I would also like to thank Dr. François Anderegg for his continuous support and guidance in all manners of laboratory techniques, Prof. Dan Dubin, Prof. Tom O'Neil, and Dr. Andrey Kabantsev for their varied perspectives, comparisons to theoretical results, and countless other contributions, and my fellow graduate students Kurt Thompson, Nicola Panzeri, I-Lin Yeh and Patrick Steinbrunner.

In the wider world of academia, I would like to thank my colleagues Roman Gerasimov, Dallar Babaian, Raj Chaklashiya, and James Wiley for their support, commentary and humor throughout my undergraduate and graduate career.

Naturally, I must also thank my family for their unwavering support, especially my parents, who have always encouraged me to reach for excellence, and done everything in their power and more to help me achieve whatever I set my mind to.

This work was supported in part by NSF Phy21-06332 and DOE DE SC0018236.

VITA

2018	B. S. in Physics *with Honors*, University of California, Los Angeles
2018-2021	Teaching Assistant, Department of Physics, University of California, San Diego
2018-2023	Research Assistant, Department of Physics, University of California, San Diego
2023	M. S. in Physics, University of California, San Diego

FIELDS OF STUDY

Major Field: Physics

Studies in Plasma Physics
Professor Patrick H. Diamond

Studies in Mechanics
Professor Daniel H. Dubin

Studies in Mathematical Physics
Professor Michael M. Fogler

Studies in Physics Estimates
Professor Thomas W. Murphy

Studies in Electrodynamics
Professor Michael M. Fogler

Studies in Statistical Mechanics
Professors Tarun Grover and Patrick H. Diamond

Studies in Quantum Mechanics
Professors Yi-Zhuang You and Massimiliano Di Ventra

Studies in Biodynamics
Professor Terence T. Hwa

PUBLICATIONS

F. Anderegg, P. Steinbrunner, J. Saret, and C.F. Driscoll, "Direct Measurement of Enhanced Particle Slowing from 1D Long-Range Collisions." APS Division of Plasma Physics Meeting Abstracts (2020).

A. Saha, J. Saret, and F. Anderegg, "Non-Linear Plasma Wave Decay to Longer Wavelengths." APS Division of Plasma Physics Meeting Abstracts (2019).

F. Anderegg, J. Saret, and C.F. Driscoll, "Test Particle Diffusion In Correlated Plasmas." APS Division of Plasma Physics Meeting Abstracts (2019).

ABSTRACT OF THE THESIS

Experimental Studies of Nonlinear Electron Acoustic Waves

by

Jacob Stone Saret

Master of Science in Physics

University of California San Diego, 2023

Professor C. Fred Driscoll, Chair

In this thesis, I discuss two related but ultimately independent courses of experimental studies in nonneutral plasma physics. The first study considers a magnesium ion plasma by examining collisions and test particle transport under magnetized and correlated conditions; the second study considers a pure electron plasma by measuring a decay of plasma waves to longer wavelength. Both of these studies include a discussion of the experimental apparatus used therein.

In the first study, I discuss collisional phenomena in a pure magnesium ion plasma and the techniques of selective spin-tagging diagnostics for the measurements of such phenomena. The experiment explores the effect of two important differences from binary collisions of bare charges: magnetization suppression, and correlation enhancement. Magnetization suppression occurs when the cyclotron orbit size r_c becomes comparable to the distance of closest approach b, giving a reduction of approximately $\log(r_c/b)$. In the opposite regime, lower temperatures quadratically increase the correlation parameter, and the same experiment shows that the collision rate increases as $\exp(-T)$.

In the second study, I consider the decay of electron acoustic waves (EAWs) in a pure electron plasma. I begin this study with a discussion of Landau damping, which quickly filters out EAWs from most plasmas; however, at large amplitudes nonlinear effects perturb the velocity distribution in such a way that Landau damping is all but eliminated, allowing for extended observation of EAWs and their decay to longer-wavelength daughter waves. Interestingly, no lower threshold for decay is observed, but instead a change in regime occurs around a drive amplitude of 0.3V, below which the growth rate of daughter waves is generally constant. For drive amplitudes above about 1V, simple decay is absent, but instead "ringing" is observed at several higher harmonics, which exhibit frequency growth due to heating effects.

Chapter 1

Introduction

Single-species, single-sign-charge plasmas, known as nonneutral plasmas, have the rare combination of confinement over long timescales in global thermal equilibrium, while being relatively straightforward to manipulate and diagnose in the laboratory. In addition, these nonneutral plasmas are a unique medium for the study of numerous physical phenomena, both in the regimes available for exploration, and the diagnostic techniques available for measurements. The physics accessible through the study of nonneutral plasmas encompasses topics ranging from basic plasma physics and transport processes to spectroscopy, astrophysics, and fusion. [1–4]

Work in this thesis focuses on two different experiments carried out on two different machines in the Nonneutral Plasma Physics group at UCSD — laser diag-

nosed test particle transport in magnesium ion plasmas on the IV apparatus, and electrically diagnosed acoustic wave evolution in electron plasmas on the EV apparatus. Both the IV and EV apparatuses are Penning-Malmberg traps containing magnesium-ion and electron plasmas, respectively.

Chapter 2 begins with a presentation of the details of the magnesium-sourced Penning-Malmberg trap known as the IV apparatus, including a discussion of the laser-based selective spin-tagging diagnostic. This diagnostic uses a frequency-tunable laser resonant with all or specific parts of the magnesium ion population. The lasers can be used to "tag" ions by changing their spin state from $S_{\pm 1/2}$ to $P_{\pm 1/2}$; or detect tagged ions through a cyclic transition between $S_{+1/2}$ and $P_{+3/2}$. By tagging only a specific portion, we can later repeatedly detect the distribution of these tagged ions at several later times.

Chapter 3 discusses the workings of the EV apparatus, a thermionic electron-sourced Penning-Malmberg trap with traditional electronic diagnostic systems. These electronic diagnostic systems consist of a collimator plate with a movable hole used to measure total particle count and a Faraday cup used to measure radial density. From there, we proceed with a discussion of plasma waves in Penning-Malmberg traps, focusing on Trivelpiece-Gould (TG) and electron acoustic waves (EAWs), with fast and slow phase velocities, respectively — $\omega_{TG} = (3 \sim 5)k_z\bar{v}$ and $\omega_{EAW} = (1.3 \sim 2)k_z\bar{v}$.

EAWs feature strong Landau damping which filters them out of most plasmas, but at large amplitudes, their nonlinear nature modifies the distribution in a way to mostly eliminate the Landau damping and allow them to persist long enough to quantify, and even observe a decay into longer wavelength daughter waves.

Chapter 2

Collisions and Test Particle Transport in Magnetized and Correlated Plasmas

2.1 Introduction

The properties of nonneutral plasmas make them a prime medium for the study of inter-particle correlations, especially regarding the effects of these correlations on the dynamics of magnetized plasmas. Here, we use the correlation parameter $\Gamma \equiv e^2/aT$ to represent the ratio of the electrostatic energy between two nearest

neighbor particles in the plasma — separated by the interparticle spacing a — to the thermal energy T. In magnesium ion plasmas, correlation parameters $10^{-5} < \Gamma < 10^{1}$ are obtained from temperatures in the range of 5×10^{-6} eV $< T < 5$ eV.

The accepted theory by Montgomery and Turner [5] for the perpendicular-to-parallel two-particle collision rate, $\nu_{\perp\parallel}$ in a magnetic field states that $\nu_{\perp\parallel} \propto \ln(\lambda_D / r_c)$. Under strong magnetization, Glinsky et. al. [6] propose an additional correction factor $\nu_{\perp\parallel} \propto I(\bar{\kappa}) \propto \exp(\bar{\kappa})^{2/5}$, which was measured by Hyatt and Beck [7, 8].

Theory from Baalrud [9] and simulation from Ott and Bonitz [10] starting from the strongly correlated regime, predict a decrease in collision rate with a form $\nu_{\perp\parallel} \propto g(\Gamma) \sim \exp(\Gamma)$.

Other experiments by Anderegg et al. [11] also measured the results of test particle diffusion and heat transport for the weakly correlated regime, which neither experiment nor numerical simulation had previously explored. Future experiments on the IV apparatus aim to clarify the intermediate regime of moderate correlation, where $10^{-1} < \Gamma < 10^{1}$.

2.2 The IV Apparatus

The IV apparatus is a Penning-Malmberg trap, outfitted with a magnesium ion source and laser diagnostic systems. The general mechanics of a more primitive

Penning-Malmberg trap are discussed in Chapter 3. The specific laser diagnostics for these experiments consist of two lasers set up to enter the plasma either axially — the "parallel" beam — or through a slice of the center of the plasma — the "perpendicular" beam, and a photon counter to measure the radiation emitted by laser-excited ions. This is discussed further in Section 2.2.2.

2.2.1 Representative IV Plasma Profile

Maintaining a consistent plasma is a crucial part of generating simple and replicable data. Ideally, the density should approximate a step function so that $n(r) \sim n\left[1 - \Theta\left(r - r_p\right)\right]$, a sample of which is shown in Figure 2.1(a). A plasma of this shape has a linearly increasing rotational velocity — that is, constant angular speed $\omega = [3.4 \times 10^4 \text{ cm/s}] \times [0.5 \text{ cm}]^{-1} = 6.4 \times 10^4 \text{ rad/s}$ — as seen in Figure 2.1(b), and near-constant temperature throughout, in Figure 2.1(c).

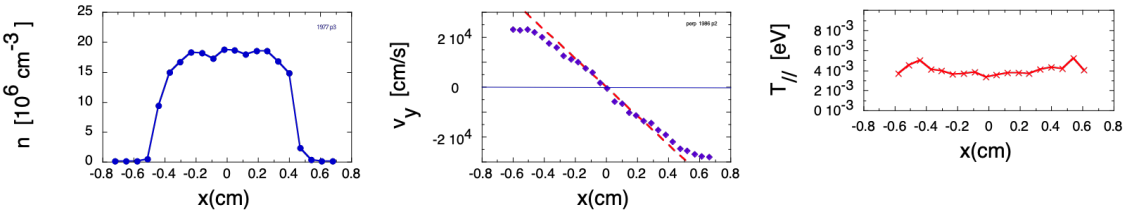

Figure 2.1: Plasma profiles for (a) density, (b) rotation, and (c) temperature. The linear fit shown on plot (b) in red shows that the rotational velocity is constant, with $f_{E\times B} = 9\text{kHz}$ and radial dimension x.

The parameters we have direct control over for these plasmas are generally density 10^5 cm^3 $< n < 10^8$ cm^3, plasma radius 0.1 cm $< r_p <$ 1 cm, plasma length 5 cm $< r_p <$ 30 cm, magnetic field 1 T $< B <$ 3 T, and temperature 5×10^{-6} eV $< T <$ 5 eV. These determine the cyclotron radius $r_c = v_{\text{th}}/\Omega_c$, impact parameter $b = e^2/T$, Debye length $\lambda_D = \sqrt{T/4\pi ne^2}$, interparticle spacing $a = (3/4\pi n)^{1/3}$, magnetic field strength $\bar{\kappa} = \sqrt{2}b/r_c$, and correlation parameter $\Gamma = e^2/aT$.

2.2.2 Selective Spin-Tagging Diagnostic

Tagging specific particles for later observation is done by using a laser to modify the orientation of the spin of the ions in the plasma, leaving the dynamics involved in particle collisions and transport unaffected. The laser can be applied either parallel or perpendicular to the magnetic field. When applied parallel, only ions at a certain radius are affected, but when applied perpendicular, all ions are affected.

The selective tagging process begins by untagging the entire population of ions — moving them to the $S_{-1/2}$ state. This is done through one optical pumping transition, by exciting them from the $S_{+1/2}$ to the $P_{-1/2}$ energy-spin state, from which they can decay back to either $S_{+1/2}$ or $S_{-1/2}$ with equal probability. By continually applying this excitement, ions which decay back to the $S_{+1/2}$ state will be re-excited and decay in the same pattern. In this way, all ions are eventually sent to the $S_{-1/2}$ state. These

three transitions are depicted in Figure 2.2(a).

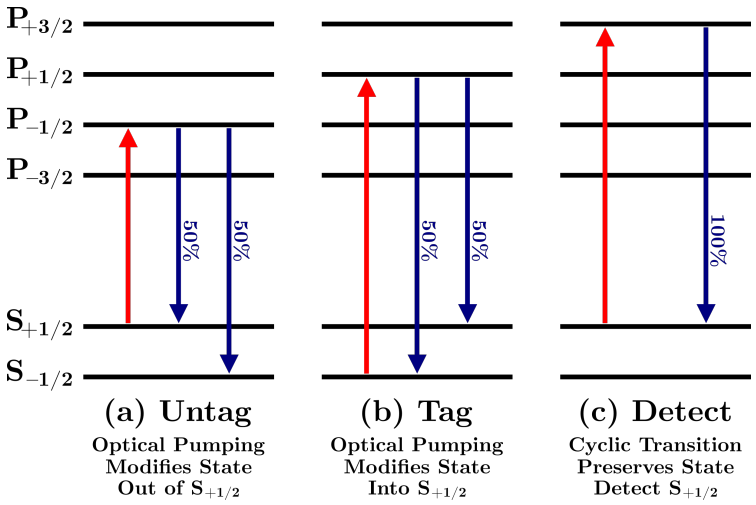

Figure 2.2: Ion spin tagging mechanics. Red arrows represent applied excitement from 280nm lasers, while blue arrows represent possible decay to lower energy states. (a) Untag optical pumping cycle applied to all ions to untag entire population. (b) Tag optical pumping cycle applied only to ions we wish to tag. (c) Cyclone transition to non-destructively detect tagged particles.

Once the whole population of ions has been untagged, a specific population can be tagged using the optical pumping cycle shown in Figure 2.2(b), which moves all affected ions to the $S_{+1/2}$ energy-spin state. As these tagged particles move about the plasma, we can exclusively excite the tagged population using the cyclone transition in Figure 2.2(c) and observe the resulting emissions to determine the distribution of tagged ions. As the cyclone transition returns the tagged particles to their original tagged state, the distribution of tagged particles can be observed at numerous times without needing to reset the population.

Chapter 3

Nonlinear Plasma Wave Decay to Longer Wavelength

3.1 Introduction

In addition to providing an excellent medium for the study of inter-particle correlations, nonneutral plasmas can be home to a wide variety of waves such as diocotron waves, Trivelpiece-Gould (TG) waves, and of particular interest to us, electron acoustic waves (EAWs). Our focus for this experiment will be the decay of EAWs with low phase velocity, which exhibit decay where the daughter waves are of longer wavelength than the initial wave. EAWs are kinetic waves existing on the low frequency

branch of electrostatic plasma waves. The behavior of these waves are generally dominated by Landau damping — a result of the velocity distribution function of the plasma — which prevents instabilities from forming, including EAWs.

The design of the EV apparatus, a Penning-Malmberg trap with a thermionic electron source, gives an initially Maxwellian distribution of trapped electrons. Launching plasma waves of moderate amplitude then flattens the velocity distribution function at the phase velocity of the wave, thus effectively eliminating Landau damping effects. This makes detailed observation of the plasma waves possible, and as they decay from an externally driven axial $m_z = 2$ mode to the double-wavelength $m_z = 1$ mode, we observe is an amplitude threshold on the $m_z = 2$ pump wave. Only when the pump wave is driven above this threshold does phase-locked exponential decay to longer wavelength occur.

3.2 The EV Apparatus

The EV machine is a Penning-Malmberg trap with a thermionic electron source, as shown in Figure 3.1. The confinement chamber consists of a traditional electron source, segmented cylindrical chamber walls, each of which may have a distinct electrical signal applied or measured. The plasma diagnostic systems consist of a collimator plate with a movable hole and Faraday cup which are used to measure

total particle count and radial density, respectively.

The electrode at the far left of Figure 3.1 generates electrons, around $N_{\text{tot}} \sim 10^9$ of which are allowed to enter the trap while the negative potential marked "Inject" is not applied to the first cylindrical segment of the wall. The electrons become axially confined in the trap when the cylinder marked "Inject" and "Dump" are both held at a large negative confinement potential $-V$. Radial confinement is achieved through an axial magnetic field B_z.

Waves are excited using a wave burst applied to the cylinder marked "Excite". Once the desired measurement has been completed, the plasma is then ejected to the right by eliminating negative potential marked "Dump". In this manner, varying the axial position and voltage of the confinement and excitement potentials, plasmas of different densities, radii and lengths may be achieved.

3.2.1 Representative EV Plasma Profile

While maintaining a consistent plasma is important on the IV apparatus, it is an especially crucial part of generating simple and replicable data on the EV machine, as the plasma is dumped from confinement after every individual experiment trial. The profile of a plasma, including its number and line densities, total particle number and radius is measured during the dump cycle of a plasma. When the confinement

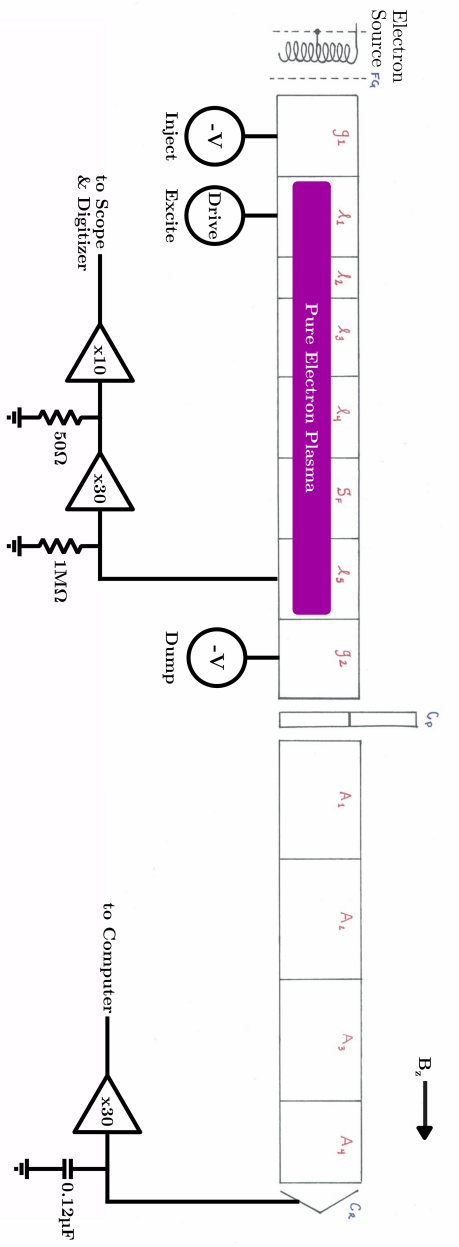

Figure 3.1: The EV apparatus, with (from left) thermionic electron source, confinement cylinders G_1-G_2, collimator plate C_P, and Faraday cup C_R. The collimator plate has a similar attachment to the one present on the Faraday cup, for measuring particle counts, not shown.

potential is removed from the cylinder marked "Dump" in Figure 3.1, many of the electrons are deposited on the collimator plate C_P immediately past this cylinder, and the remainder are deposited on the Faraday cup C_R at the far end, and the number of particles deposited on each cam be calculated. By rotating the collimator plate over several measurements of plasmas injected under identical conditions, a radial profile can be recorded, and plasma densities and potentials may be determined. A sample plasma profile is shown in Figure 3.2.

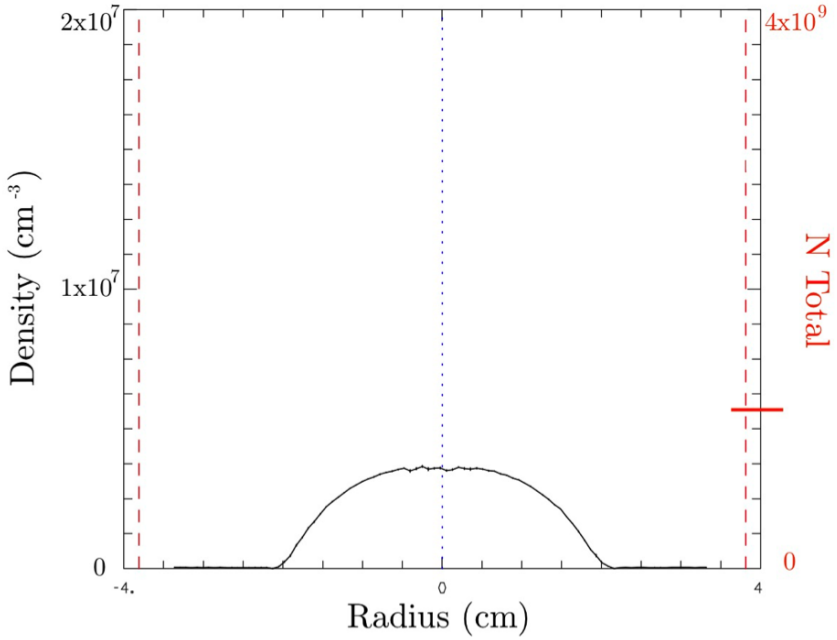

Figure 3.2: Representative profile of a pure electron plasma confined in the EV apparatus. N_{total} is depicted on the right vertical scale in red.

In this representative profile, we note that there are a total of $N_{\text{total}} = 1.14 \times 10^9$ electrons, the line density is $N_L = 3.26 \times 10^7 \text{cm}^{-1}$, the plasma radius is $R_p = 1.8\text{cm}$, and the potential at the center is $\phi(r = 0) = 10.7\text{V}$. While the wall radius of the apparatus is fixed at $R_w = 3.81\text{cm}$, the length of the plasma may be varied discretely by applying the confinement potentials to different cylindrical segments.

3.3 Plasma Waves in Penning-Malmberg Traps

Once we have ensured our plasma will be well-behaved for the duration of its confinement, various waves may be excited in the plasma through signals applied to the cylinder marked "Excite" in Figure 3.1. For example, applying a negative voltage to one of the cylinders will push electrons away from that axial position in the plasma, reducing its local density. As such, driving a cylinder at the appropriate axial position in the plasma with a voltage oscillating at the resonant frequency of a wave of interest will quickly excite standing waves, including the EAWs we are concerned with in this chapter.

Before we can delve into the decay mechanics, we must first discuss the basic parameters of the plasma waves we will be observing. One category of waves we have are Trivelpiece-Gould waves, which have a fast phase velocity, [12]

$$\omega_{TG} = \omega_p \frac{k_z}{\sqrt{k_z^2 + k_\perp^2}} \text{ which can be estimated as } (3 \sim 5) k_z \bar{v}, \tag{3.1}$$

where $k_z = \pi m_z / L_p$ with $m_z \in \mathbb{N}$, $\omega_p = \sqrt{4\pi n e^2 / m}$, and thermal velocity $\bar{v}$.

On the other hand, we have EAWs, which have a slow phase velocity, which can be estimated as $\omega_{EAW} = (1.3 \sim 2) k_z \bar{v}$, with the perpendicular wavenumber given by

$$k_\perp = \frac{1}{R_p} \sqrt{\frac{2}{\log(R_w / R_p)}}, \tag{3.2}$$

when the plasma radius is not near the wall radius [13,14]. In addition, EAWs exhibit strong Landau damping which quickly filters them out when excited in most plasmas. At large wave amplitudes, the nonlinear nature of EAWs traps particles moving near the phase velocity of the wave, causing a flattened segment in the particle velocity distribution as shown in Figure 3.3.

This modified distribution function significantly reduces the effects of Landau damping. As we discussed in the introduction to this chapter, this allows waves in the plasma to remain at observable amplitudes for significantly longer durations. Without reducing Landau damping, we would be unable to observe the longer timescale wave effects — including the decay to longer wavelength daughter waves [15, 16].

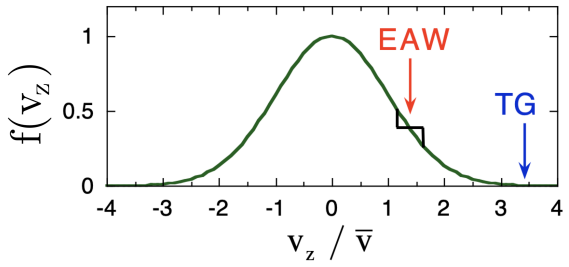

Figure 3.3: Change in velocity distribution function of electrons when waves are excited in the plasma. EAWs and TG waves have phase velocities in the respective regions indicated.

3.4 Experimental Measurements of Wave Decay

As we saw in the previous section, we have theoretical predictions for the frequencies of EAW modes in our plasma. Using this, we can apply a driver of an amplitude-rounded burst of about 100 cycles to one of the EV cylinders, to excite a high-amplitude EAW. This burst-based excitement induces the flattened velocity distribution required to eliminate Landau damping as discussed above. From here, we observe the waves in the plasma response once the burst has ended, an example of which is presented in Figure 3.4.

Now that we have generated EAWs in our plasma, we can compare their frequencies and wavenumbers to the established theoretical dispersion relation to distinguish excited TG modes and excited EAW modes. Such a comparison for several modes in two different plasma lengths is shown in Figure 3.5.

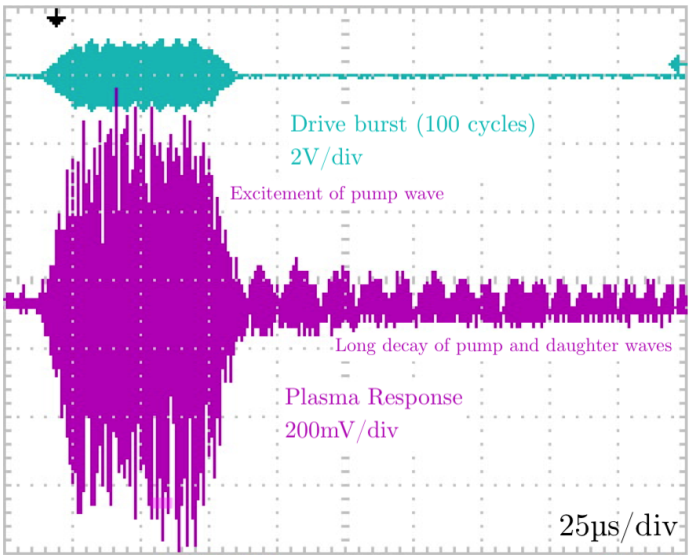

Figure 3.4: An example of a $\sim$ 100 cycle drive burst exciting EAWs in a plasma, and the plasma's response measured on a separate cylinder.

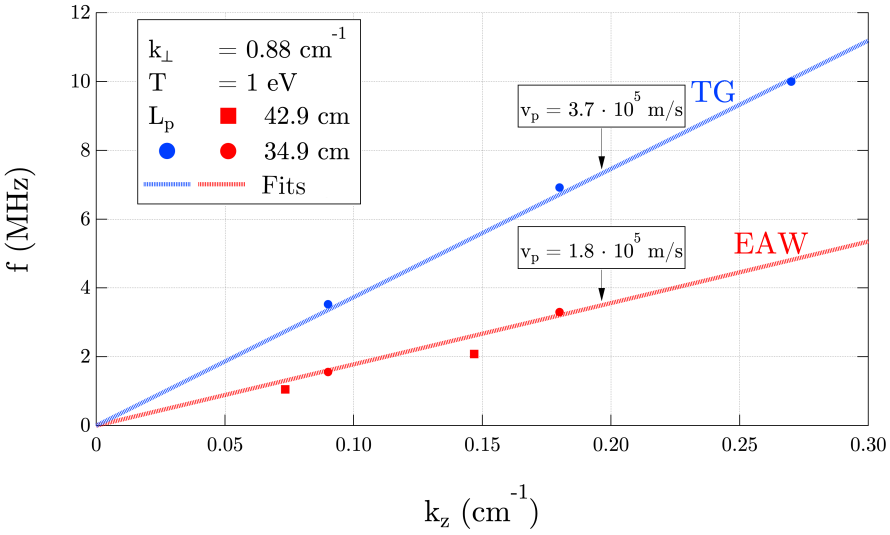

Figure 3.5: Frequency and wavenumber comparison to phase velocity.

3.4.1 Low Drive Regime

Having successfully identified our directly excited pump waves for any amplitude, we can look for energy decay to daughter waves. In the low drive amplitude regime, where $V_{\text{drive}} < 1V_{\text{pp}}$, we observe the excitement of daughter waves, and take time-binned Fourier transformations to generate a time-frequency-amplitude plot of the plasma response — shown in purple in Figure 3.4. This time-frequency-amplitude plot is displayed in Figure 3.6, which shows the direct excitement of a pump EAW at 2.75MHz, and subsequent growth of a daughter wave at 1.03MHz shortly after the end of the burst.

Translating this data from time-frequency space to time-amplitude space, Figure 3.7 displays the direct excitement of a pump EAW at 2.75MHz. Modulational instabilities in higher-frequency EAW modes cause subsequent growth of daughter waves. In this case, we observe such a daughter wave at a frequency of 1.03MHz shortly after the end of the burst, demonstrating the decay to longer wavelength through this parametric resonance phenomena.

More tests of the growth of daughter waves in the low drive amplitude regime show us how the amplitude of the pump wave determines the growth rate, and the decay threshold below which daughter waves are not excited, shown in Figure 3.8.

While this data demonstrates a change in growth behavior, as illustrated by the

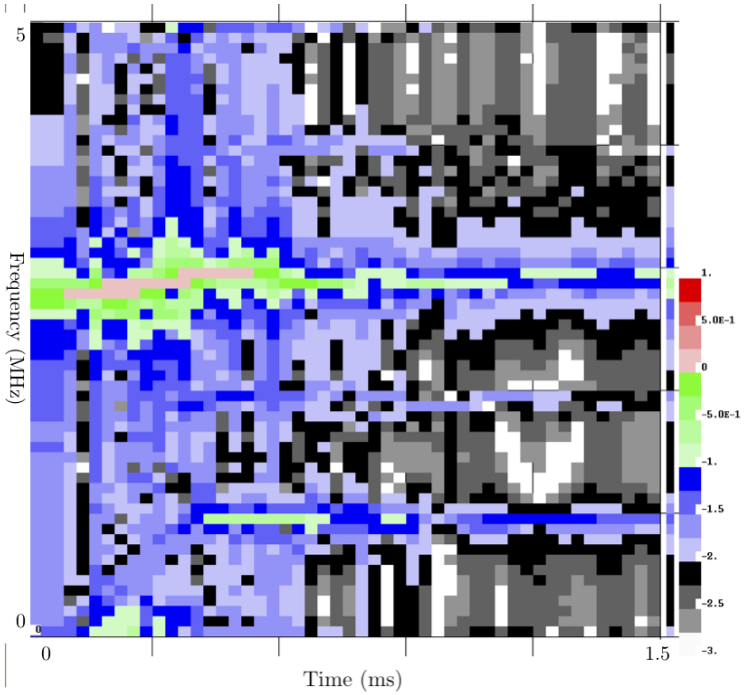

Figure 3.6: Direct excitement of pump wave and subsequent growth of daughter wave. Frequency is on the vertical axis at left, time is on the horizontal axis, and amplitude is represented in a logarithmic scale by the colors on the scale at right.

linear increase in growth rate above a drive amplitude of 0.3V, there is no clear lower threshold for decay, as daughter waves are still excited with a consistent growth rate by pump waves driven with amplitude below 0.3V. Since we have shown there is regular decay to longer wavelength in the low drive regime, our next step is to examine a possible upper amplitude threshold by moving to the high drive regime.

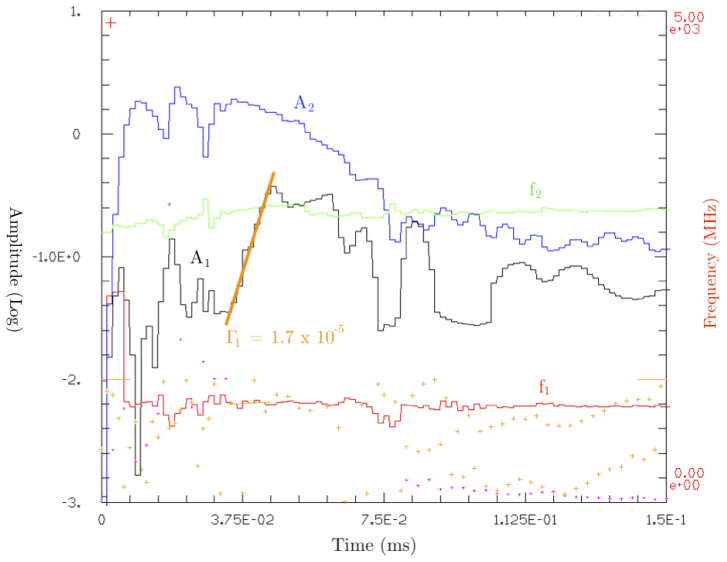

Figure 3.7: Amplitude A_1 and growth rate $\Gamma_1 = 170 \times 10^3 \mathrm{s}^{-1}$ of the daughter wave (EAW $m_z = 1$) are shown in black and orange, respectively. Frequencies of the pump wave (EAW $m_z = 2$, $f_2 = 3.0$MHz) and daughter wave (EAW $m_z = 1$, $f_1 = 0.96$MHz) are shown in green and red, respectively.

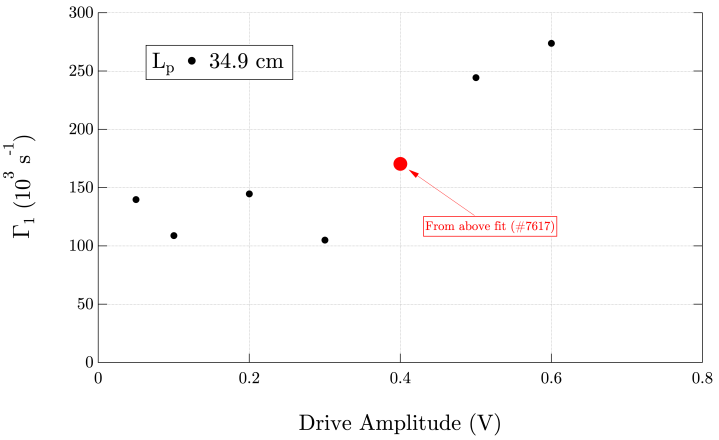

Figure 3.8: Dependence of daughter wave growth rate Γ_1 on pump wave drive amplitude, which determines excitation amplitude A_2. The highlighted data point was generated from the data shown in Figure 3.7.

3.4.2 High Drive Regime

In contrast to the low drive regime, pump waves generated by a drive signal above 1V in amplitude remain stable and do not excite any longer-wavelength daughter waves, but instead "ring" at multiple higher harmonics with temporal frequency growth due to heating effects from these high-frequency daughter waves. An example of this high-amplitude pump wave and decay is shown in Figure 3.9.

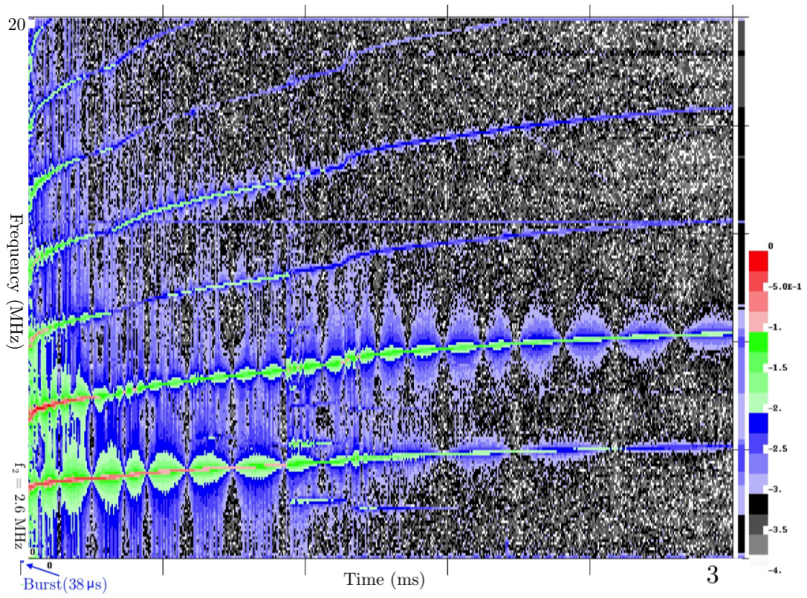

Figure 3.9: High drive regime and "ringing" at high-frequency harmonics with temporal frequency growth from heating effects. Colors are logarithmic in amplitude as shown by the scale at right.

References

[1] R. C. Davidson, Physics of Nonneutral Plasmas, vol. 5. Addison-Wesley New York, 1990.

[2] S. I. Braginskii, Transport Processes in a Plasma. RvPP, 1965.

[3] R. S. Van Dyck, D. L. Farnham, and P. B. Schwinberg, "Tritium–helium-3 mass difference using the penning trap mass spectroscopy," Phys. Rev. Lett., vol. 70, pp. 2888–2891, May 1993.

[4] F. L. Hinton and R. D. Hazeltine, "Theory of plasma transport in toroidal confinement systems," Rev. Mod. Phys., vol. 48, pp. 239–308, Apr 1976.

[5] D. Montgomery, L. Turner, and G. Joyce. Magnetic field dependence of plasma relaxation times. Physics of Fluids, 17(12):954, Jan 1974.

[6] M. Glinsky, T. O'Neil, and M. Rosenbluth. Collisional equipartition rate for a magnetized pure electron plasma. Physics of Fluids B: Plasma Physics 4, 1156 (1992).

[7] A. W. Hyatt, C. F. Driscoll, and J. H. Malmberg. Measurement of the Anisotropic Temperature Relaxation Rate in a Pure Electron Plasma Phys. Rev. Lett. 59, 2975 (1987).

[8] B.R. Beck, J. Fajans and J.H. Malmberg. Measurement of Collisional Anisotropic Temperature Relaxation in a Strongly Magnetized Pure Electron Plasma. Phys. Rev. Lett. 68, 317 (1992).

[9] S.D. Baalrud. Transport coefficients in strongly coupled plasmas. Physics of Plasmas 19.3 (2012).

[10] T. Ott and M. Bonitz. Diffusion in a Strongly Coupled Magnetized Plasma. Phys. Rev. Lett. 107, 135003, Sep 2011.

[11] F. Anderegg, D. H. E. Dubin, M. Affolter and C. F. Driscoll. Measurements of correlations enhanced collision rates in the mildly correlated regime ($\Gamma \sim 1$). Physics of Plasmas 24, 092118 (2017).

[12] J.P. Holloway and J.J. Dorning. Undamped plasma waves. Phys. Rev. A 44, 3856 (1991).

[13] F. Anderegg, C. F. Driscoll, D. H. Dubin, T. M. O'Neil, and F. Valentini. Electron acoustic waves in plasma. Phys. Plasmas 16, 055705 (2009).

[14] F. Anderegg, C. F. Driscoll, D. H. E. Dubin, and T. M. O'Neil. Wave-Particle Interactions in Electron Acoustic Waves in Pure Ion Plasmas. Phys. Rev. Lett. 102, 095001 (2009)

[15] L. D. Landau. On the vibrations of the electronic plasma. J. Phys. Moscow 10, 25 (1946).

[16] I. B. Bernstein, J. M. Green, and M. D. Kruskal. Exact nonlinear plasma oscillations. Phys. Rev. 108, 546 (1957).